

# Dynamics of Space Elevator after Tether Rupture

Vladimir S. Aslanov<sup>1</sup> and Alexander S. Ledkov<sup>2</sup>  
*Samara State Aerospace University, Samara, 443086, Russian*

Arun K. Misra<sup>3</sup>  
*McGill University, Montreal, H3A 2K6, Canada*

and  
Anna D. Guerman<sup>4</sup>  
*University of Beira Interior, Covilhã, Portugal*

**This paper presents a study of space elevator dynamics after the tether rupture due to its collision with a piece of space debris. The flexible heavy tether is modeled by a set of massive points connected by massless viscous bars. The tether is assumed to break at the geostationary orbit; its consequent motion is subject to gravitational and aerodynamic forces. Numerical simulation shows that, after entering the atmosphere, the majority of the tether segments are broken down by aerodynamic forces and smoothly descend to the Earth's surface. This process is accompanied by formation of large loops, some of which can get beyond the atmosphere. Meanwhile, some parts of the tether reach the surface of the Earth with considerable speed, jeopardizing both spaceborne and ground objects in the equatorial plane.**

## Nomenclature

$C_n$  = dimensionless coefficient of the normal aerodynamic force

$C_\tau$  = dimensionless coefficient of the tangential aerodynamic force

$D_i$  = coefficient of internal friction for longitudinal oscillations of the  $i$ -th tether segment, kg-m/s

---

<sup>1</sup>Head of Theoretical Mechanics Department, Samara State Aerospace University, Theoretical Mechanics Department, Russia, Samara, Moskovskoye Shosse 34, 443086.

<sup>2</sup>Associate professor, Samara State Aerospace University, Theoretical Mechanics Department, Russia, Samara, Moskovskoye Shosse 34, 443086.

<sup>3</sup>Thomas Workman Professor and Chairman, McGill University, Department of Mechanical Engineering, 817 Sherbrooke Street West, Montreal, QC, Canada H3A 2K6, AIAA Fellow.

<sup>4</sup>Associate Professor, Coordinator of the Centre for Aerospace Science and Technologies, University of Beira Interior, Dept. of Electromechanical Engineering, Portugal, Covilhã, Calçada Fonte do Lameiro 6200-001, AIAA Senior Member.

- $d_T$  = diameter of the tether, m  
 $E$  = modulus of elasticity of the tether, Pa  
 $\mathbf{F}_{Ai}$  = vector of aerodynamic force at point  $P_i$ , N  
 $\mathbf{F}_{FRi}$  = vector of friction force at point  $P_i$ , N  
 $\mathbf{F}_\perp$  = projection of the resultant force onto the tangent plane, N  
 $\mathbf{G}_i$  = vector of gravitational force at point  $P_i$ , N  
 $L_0$  = length of the unstrained tether, m  
 $l_i$  = length of the unstrained i-th segment of tether, m  
 $M_\infty$  = Mach number of the undisturbed flow  
 $m_i$  = mass of i-th tether's particle, m  
 $\mathbf{N}_{j,i}$  = normal component of aerodynamic force at the j-th part of i-th tether's section, N  
 $q_i$  = dynamic pressure at point  $P_i$ , Pa  
 $\mathbf{R}_i$  = vector of the normal reaction of the Earth surface at point  $P_i$ , N  
 $r_{cm}$  = distance from the center of the Earth to the center of mass of the top part of the elevator, m  
 $r_i$  = radial distance of i-th tether's particle from the center of the Earth, m  
 $r_{GEO}$  = radius of the geosynchronous orbit, m  
 $S_i$  = area of cross-section of the i-th tether part, m<sup>2</sup>  
 $S_{j,i}$  = area of the longitudinal section of the j-th part of i-th tether section, m<sup>2</sup>  
 $T$  = kinetic energy, J  
 $\mathbf{T}_i$  = vector of the tension in the tether sections  $P_{i-1}P_i$ , N  
 $V_{cm}$  = absolute velocity of the center of mass of the top part of the elevator, m/s  
 $\mathbf{V}_i$  = velocity vector of point  $P_i$ , m/s  
 $V_p$  = parabolic velocity, m/s  
 $V_{xi}, V_{yi}, V_{zi}$  = components of the velocity vector of the i-th point in  $OXYZ$  reference frame, m/s  
 $W$  = potential energy, J

- $\mathbf{X}_A$  = aerodynamic drag, N  
 $X_i, Y_i, Z_i$  = coordinates of the i-th point in  $OX_iY_iZ_i$  reference frame, m  
 $x_i, y_i, z_i$  = coordinates of the i-th point in  $OXYZ$  reference frame, m  
 $\mathbf{Y}_A$  = aerodynamic drag, N  
 $\alpha_{j,i}$  = angle between vectors  $\mathbf{p}_{i+1}$  and  $\mathbf{V}_i$  for j-th part of i-th tether section, rad  
 $\gamma_i$  = elongation of the i-th tether section  
 $\Delta L_i$  = length of the i-th tether section, m  
 $\eta$  = loss factor, m  
 $\kappa$  = adiabatic index of environment  
 $\mu$  = gravitational constant of the Earth,  $\text{m}^3/\text{s}^2$   
 $\mu_s$  = coefficient of sliding friction on the Earth surface  
 $\mu_r$  = coefficient of static friction on the Earth surface  
 $\rho_{at}$  = atmospheric density at point  $P_i$ ,  $\text{kg}/\text{m}^3$   
 $\rho_i$  = length of the i-th section of deformed tether, m  
 $\tau_{j,i}$  = tangential component of aerodynamic force at the j-th part of i-th tether section, N  
 $\Phi_i^C$  = vector of Coriolis force at point  $P_i$ , N  
 $\Phi_i^{cf}$  = vector of centrifugal force at point  $P_i$ , N  
 $\Phi_i^{rot}$  = vector of Euler force of inertia at point  $P_i$ , N  
 $\omega_E$  = angular velocity of the Earth, rad/s

## I. Introduction

Building a space elevator is supposed to decrease drastically the cost of cargo delivery into space avoiding expensive launchers. This project attracts nowadays attention of many members of space community, from engineers and scientists to environmentalists and lawyers, as well as potential investors all over the world [1, 2]. The

main idea behind most of space elevator proposals is to tether a base point at the Earth equator to a counterweight located beyond the geostationary orbit and to deliver payload to space by one or several climbers [3]. The first description of such structure appears as early as in 1960 [4], though the first rigorous studies are published a few years later [5, 6]. Their authors have used simple mathematical models to estimate the necessary strength of the space elevator's ribbon material. Pearson, in his fundamental study on the matter [7], investigates natural frequencies of the space elevator as a function of the system parameters and proposes a formula to calculate the cross section of the tether depending on the strength of the material, the planet mass, and the angular velocity of its rotation. His estimate for the upper limit for the length of an Earth space elevator rounds 144 000 km [7]. Towards the end of the 20th century, NASA has funded several projects to develop technologies for the construction of space elevator; one of these projects has been led by Edwards. Several researchers have developed various designs of the space elevator based on contemporary technologies and identified the milestones for creation of the first space elevator. In his final report published in 2003, Edwards concludes that development of a space elevator would take 15 years [8]. Despite Edwards' optimism, there are still several scientific and technologic issues waiting to be solved. Many researchers point out that the main obstacle for building a space elevator is the lack of sufficiently strong tether material [9, 10]. Another major challenge is to ensure survival of the structure. In the circumterrestrial space there is a large number of different-size moving objects which pose a serious threat to the relatively brittle tether. According to some experts, small space particles have caused the failures of SEDS-2 (1994) and TSS-1R (1996) experiments. By estimations of Edwards, space elevator would collide with meteorites with diameters more than 0.1 m at least once a year; a tether with diameter of several centimeters is likely to be destroyed within a week [11].

The above problems, along with several other issues, such as tether deployment strategy [12] and tether/climber motion stabilization [13, 14], must be studied while developing a space elevator with more complex structure. Here we focus on one of the aspects that concerns safety of space elevator exploration and consider system dynamics after an eventual tether rupture.

Destruction of a space tether due to collision with space debris is quite a probable scenario. Some aspects of a space tether system failure due to the tether rupture have been studied before, e.g., Bergamaschi [15] has studied tether motions after catastrophic failure of the cable linking a tethered subsatellite to the Shuttle. However, the

problem of space elevator destruction by space debris has not been considered yet in sufficient details. Most projects take it for granted that the tether, being rather thin, would safely burn in the atmosphere.

The aim of this paper is to study the post-failure motion of a space elevator. We develop a mathematical model that takes into account the influence of aerodynamic forces and perform numerical analysis of the system dynamics. The study of behavior for the upper and lower parts of the elevator is done assuming that the tether rupture occurs in the vicinity of the geostationary orbit. Our analysis shows that the elements of the destroyed elevator can be a serious threat for both spaceborne and ground objects.

## **II. Mathematical model for the dynamics of space elevator**

### **A. General remarks**

Consider a space elevator that consists of a tether of circular cross-section and a counterweight attached to the tether at its end. The system is deployed in the equatorial plane. Motion of any climber (cage) along the tether is not considered here.

Mathematical model of motion of the space elevator after its destruction should take into account a number of important features. First, during the fall the tether is stretched unevenly and can contain loose parts. Secondly, the shape of the tether may considerably differ from a straight line. Thirdly, the tether's interaction with the atmosphere has significant influence on the system dynamics.

A model of a tether as a heavy, thick, flexible string most adequately describes the physics of the process. It allows one to obtain the most accurate results, but its use is associated with considerable computing difficulties [16]. Therefore within the limited scope of this paper a simpler model that requires less computing resources is constructed. In this model, the tether is represented as a set of massive points connected by massless viscoelastic bars. When the number of points tends to infinity, the model describes a heavy flexible string; when the number of points is zero, one gets an elastic bar. This model has been used for the analysis of abnormal situations during implementation of YES-2 project [17, 18]. A similar model is presented in [19]; however, it does not account for the atmospheric influence, making impossible its utilization for analysis of the space elevator's fall.

## B. Model of the tether

The tether is divided into  $N$  segments  $\Delta L_i$  ( $i = \overline{1, N}$ ) (Fig. 1) and each section is modeled by a particle  $P_i$  with mass  $m_i$ . The forces between two neighboring segments  $\Delta L_i$  and  $\Delta L_{i+1}$  are modeled by a viscoelastic interaction of points  $P_i$  and  $P_{i+1}$ , namely, by systems of spring and damper with stiffness and viscosity equal to those of the corresponding parts of the actual tether. That is, at each point  $P_i$  the forces  $T_i$  and  $T_{i+1}$  are equal to the tensions in the tether sections  $P_{i-1}P_i$  and  $P_iP_{i+1}$  respectively. The point  $P_0$  is fixed on the surface of the Earth and the point  $P_{N+1}$  corresponds to the counterweight. The section  $P_{i-1}P_i$  of the tether is called the  $i$ -th section.

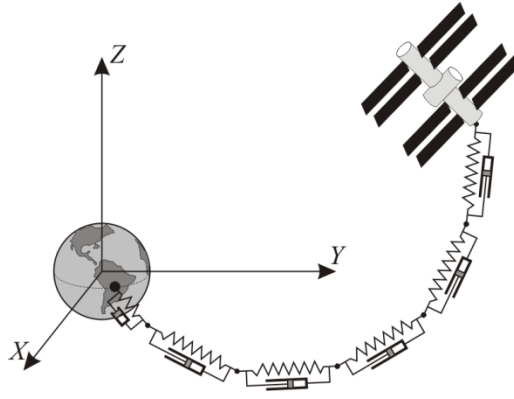


**Fig. 1 Multipoint model of the space elevator**

## C. Vector equations of motion for the tether segments

To obtain the equations of motion, we use a rotating Greenwich coordinate frame  $OXYZ$ . Point  $O$  is the center of mass of the Earth, the plane  $OXY$  coincides with the equatorial plane, the axis  $OX$  is directed to the Greenwich meridian, the axis  $OZ$  lies along the spin axis of the Earth, and  $OY$  completes the right-hand system. This system rotates about axis  $OZ$  with constant angular velocity  $\omega_E$ .

Point  $P_i$  is subject to the following forces: gravitational force  $\mathbf{G}_i$ , aerodynamic force  $\mathbf{F}_{Ai}$ , tensions from the neighboring parts  $\mathbf{T}_i$  and  $-\mathbf{T}_{i+1}$ , and the forces of inertia caused by rotation of the coordinate system, i.e., centrifugal force  $\Phi_i^{cf}$  and Coriolis force  $\Phi_i^C$  (Fig. 2). As the Earth rotates with constant angular velocity, the Euler force of inertia vanishes:  $\Phi_i^{rot} = 0$ . One can write down the Newton second law for non-inertial system  $OXYZ$  in the form:

$$m_i \ddot{\mathbf{r}}_i = \mathbf{G}_i + \mathbf{F}_{A_i} + \mathbf{T}_i - \mathbf{T}_{i+1} + \Phi_i^{cf} + \Phi_i^C \quad (1)$$

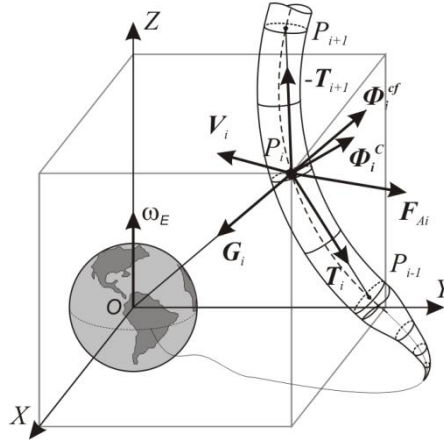


**Fig. 2 Forces operating on the point**

We assume that the gravitational field of the Earth is Newtonian; in this case, the vector of the gravitational force at  $P_i$  has the form

$$\mathbf{G}_i = \left[ -\frac{\mu m_i}{r_i^3} x_i, -\frac{\mu m_i}{r_i^3} y_i, -\frac{\mu m_i}{r_i^3} z_i \right]^T, \quad (2)$$

To more accurately account for the gravitational field of the Earth, one can replace (2) by a more evolved potential represented as a series of spherical functions [20].

The tether segments are subject to the forces of inertia caused by rotation of the Earth. The centrifugal force of inertia can be calculated as

$$\Phi_i^{cf} = -m_i \boldsymbol{\omega}_E \times (\boldsymbol{\omega}_E \times \mathbf{r}_i),$$

where  $\boldsymbol{\omega}_E = [0, 0, \omega_E]^T$  is angular velocity of the Earth rotation in the  $OXYZ$  coordinate system. The Coriolis force of inertia can be found as

$$\boldsymbol{\Phi}_i^C = -2m_i\boldsymbol{\omega}_E \times \mathbf{V}_i.$$

In  $OXYZ$  system the vectors  $\boldsymbol{\Phi}_i^{cf}$  and  $\boldsymbol{\Phi}_i^C$  have components

$$\begin{aligned}\boldsymbol{\Phi}_i^{cf} &= [m_i\omega_E^2 x_i; m_i\omega_E^2 y_i; 0]^T, \\ \boldsymbol{\Phi}_i^C &= [2m_i\omega_E \dot{y}_i; -2m_i\omega_E \dot{x}_i; 0]^T.\end{aligned}\tag{3}$$

#### D. Tension in the tether

The tension force vector is directed along the vector  $\boldsymbol{\rho}_i$  and has components:

$$\mathbf{T}_i = \left[ T_i \frac{x_{i-1} - x_i}{\rho_i}; T_i \frac{y_{i-1} - y_i}{\rho_i}; T_i \frac{z_{i-1} - z_i}{\rho_i} \right]^T,\tag{4}$$

where  $\rho_i = \sqrt{(x_i - x_{i-1})^2 + (y_i - y_{i-1})^2 + (z_i - z_{i-1})^2}$ . For the end segments  $T_0 = T_{N+2} = 0$ . The tension in the  $i$ -th tether segment can be found from the following relations [16]:

$$T_i = \begin{cases} ES_i(\gamma_i - 1) + D_i \frac{\partial \gamma_i}{\partial t}, & \gamma_i > 1, \\ 0, & \gamma_i \leq 1, \end{cases}\tag{5}$$

where  $\gamma_i = \rho_i / l_i$ ,  $\rho_i = |\mathbf{r}_i - \mathbf{r}_{i-1}|$ ,  $D_i = \sqrt{\frac{ES_i m_i}{l_i}} \eta$  [16].

### E. The aerodynamic forces acting on the tether segment

To determine the aerodynamic force acting on tether segments connected at the point  $P_i$ , one can represent each segment as a cylindrical rod bent in the middle (Fig. 3). For calculation of the aerodynamic forces, for simplicity, it was assumed that halves of tether segments  $\rho_i$  and  $\rho_{i+1}$  adjacent to the point  $P_i$  move translationally with the velocity of this point [21]. The tether segments are supposed to be quite small, so that the atmosphere density along each one of them is constant.

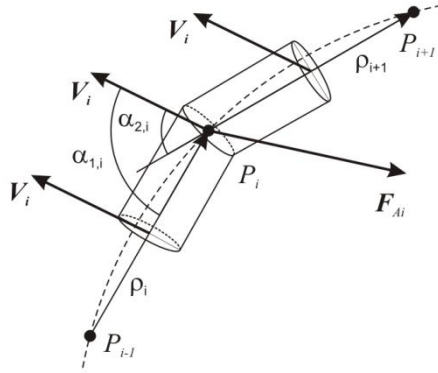


**Fig. 3 The aerodynamic forces at i-th part of the tether**

Consider one of the above cylindrical rods (Fig. 4). During its motion in the atmosphere, the rod is subject to the aerodynamic force with a normal component  $N_{2,i}$  and tangential component  $\tau_{2,i}$ . Vector  $\tau_{2,i}$  is directed along the rod and can be calculated as

$$\tau_{2,i} = C_t S_{2,i} q_i \frac{\rho_{i+1}}{\rho_{i+1}}, \quad (6)$$

where  $S_{2,i} = d_r \rho_{i+1} / 2$ . Vector  $N_{2,i}$  is perpendicular to vector  $\rho_{i+1}$  and lies in the plane formed by vectors  $V_i$  and  $\rho_{i+1}$ . The modulus of this vector is

$$N_{2,i} = C_n S_{2,i} q_i.$$

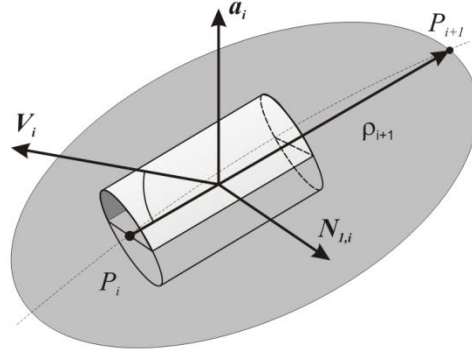


**Fig. 4 Interaction of the tether segment with the atmosphere**

To obtain the aerodynamic characteristics of the tether, one can use the method based on the Newtonian shock theory. For the case of hypersonic flow of a body in the rarefied atmosphere, this method provides good matching between the calculated and experimental data. For the cylinder one obtains the following relations [22]:

$$C_r = 0, C_n(\alpha) = \frac{2}{3} k \sin^2 \alpha, \quad (7)$$

where the coefficient  $k$  depends on the velocity and atmospheric parameters:

$$k = \frac{2}{\kappa M_\infty^2} \left[ \left( \frac{\kappa+1}{2} M_\infty^2 \right)^{\frac{\kappa}{\kappa-1}} \cdot \left( \frac{\kappa+1}{2\kappa M_\infty^2 - \kappa + 1} \right)^{\frac{1}{\kappa-1}} - 1 \right].$$

Then

$$N_{2,i} = C_n S_{2,i} \frac{\rho_{ai} V_i^2}{2} = \frac{\rho_{ai} V_i^2 k d_T \rho_{i+1}}{6} \sin^2 \alpha_{2,i}.$$

To express the vector  $\mathbf{N}_{2,i}$  in terms of  $\mathbf{V}_i$  and  $\boldsymbol{\rho}_{i+1}$ , one can notice that the vector  $\mathbf{a}_{2,i} = \mathbf{V}_i \times \boldsymbol{\rho}_{i+1}$  is orthogonal to both  $\mathbf{V}_i$  and  $\boldsymbol{\rho}_{i+1}$  and  $|\mathbf{a}_{2,i}| = V_i \rho_{i+1} \sin \alpha_{2,i}$ . Cross product of  $\mathbf{a}_{2,i}$  with  $\boldsymbol{\rho}_{i+1}$  gives the vector  $\mathbf{n}_{2,i}$  which direction coincides with that of  $\mathbf{N}_{2,i}$ , and

$$|\mathbf{n}_{2,i}| = a_{2,i} \rho_{i+1} \sin \frac{\pi}{2} = V_i \rho_{i+1}^2 \sin \alpha_{2,i}.$$

Taking into account the above expression, the vector  $\mathbf{N}_{2,i}$  can be represented as

$$\mathbf{N}_{2,i} = \frac{\rho_{ai} V_i k d_T}{6 \rho_{i+1}} \sin \alpha_{2,i} \mathbf{n}_{2,i} = \frac{\rho_{ai} V_i k d_T}{6 \rho_{i+1}} \sin \alpha_{2,i} (\mathbf{V}_i \times \boldsymbol{\rho}_{i+1}) \times \boldsymbol{\rho}_{i+1}.$$

A similar expression can be obtained for the other cylinder:

$$\mathbf{N}_{1,i} = \frac{\rho_{ai} V_i k d_T}{6 \rho_i} \sin \alpha_{1,i} (\mathbf{V}_i \times \boldsymbol{\rho}_i) \times \boldsymbol{\rho}_i. \quad (8)$$

Now one obtains the principal vector of the aerodynamic forces at the tether segment:

$$\mathbf{F}_{Ai} = \mathbf{N}_{1,i} + \mathbf{N}_{2,i} + \boldsymbol{\tau}_{1,i} + \boldsymbol{\tau}_{2,i}. \quad (9)$$

To determine the angles  $\alpha_{1,i}$  and  $\alpha_{2,i}$  we need to use the formula of the modulus of the scalar products:

$$\cos \alpha_{1,i} = \frac{\mathbf{V}_i \cdot \boldsymbol{\rho}_i}{V_i \rho_i}, \quad \cos \alpha_{2,i} = \frac{\mathbf{V}_i \cdot \boldsymbol{\rho}_{i+1}}{V_i \rho_{i+1}}.$$

Taking into account (6)-(8),  $\tau_{j,i} = 0$  vanish and equation (9) can be written in the form

$$\mathbf{F}_{Ai} = \mathbf{N}_{1,i} + \mathbf{N}_{2,i} = \frac{\rho_{ai} V_i k d_T}{6} \left( \frac{\sin \alpha_{1,i}}{\rho_i} \mathbf{n}_{i,i} + \frac{\sin \alpha_{2,i}}{\rho_{i+1}} \mathbf{n}_{i,i+1} \right), \quad (10)$$

where

$$\mathbf{n}_{i,j} = \begin{bmatrix} [(x_j - x_{j-1})\dot{z}_i - (z_j - z_{j-1})\dot{x}_i](z_j - z_{j-1}) - [(y_j - y_{j-1})\dot{x}_i - (x_j - x_{j-1})\dot{y}_i](y_j - y_{j-1}) \\ [(y_j - y_{j-1})\dot{x}_i - (x_j - x_{j-1})\dot{y}_i](x_j - x_{j-1}) - [(z_j - z_{j-1})\dot{y}_i - (y_j - y_{j-1})\dot{z}_i](z_j - z_{j-1}) \\ [(z_j - z_{j-1})\dot{y}_i - (y_j - y_{j-1})\dot{z}_i](y_j - y_{j-1}) - [(x_j - x_{j-1})\dot{z}_i - (z_j - z_{j-1})\dot{x}_i](x_j - x_{j-1}) \end{bmatrix}.$$

#### F. The scalar equations of motion for tether points

Substituting (2)-(4) and (10) into (1), one arrives at the system of equations for motion of the  $i$ -th point of the elevator:

$$\begin{aligned} \frac{dx_i}{dt} &= V_{xi}, \\ \frac{dy_i}{dt} &= V_{yi}, \\ \frac{dz_i}{dt} &= V_{zi}, \\ \frac{dV_{xi}}{dt} m_i &= -\frac{\mu m_i}{r_i^3} x_i + F_{Aix} + T_i \frac{x_i - x_{i-1}}{\rho_i} - T_{i+1} \frac{x_{i+1} - x_i}{\rho_{i+1}} + m_i \omega_3^2 x_i + 2m_i \omega_3 V_{yi}, \\ \frac{dV_{yi}}{dt} m_i &= -\frac{\mu m_i}{r_i^3} y_i + F_{Aiy} + T_i \frac{y_i - y_{i-1}}{\rho_i} - T_{i+1} \frac{y_{i+1} - y_i}{\rho_{i+1}} + m_i \omega_3^2 y_i - 2m_i \omega_3 V_{xi}, \\ \frac{dV_{zi}}{dt} m_i &= -\frac{\mu m_i}{r_i^3} z_i + F_{Aiz} + T_i \frac{z_i - z_{i-1}}{\rho_i} - T_{i+1} \frac{z_{i+1} - z_i}{\rho_{i+1}}. \end{aligned} \quad (11)$$

### G. Motion of a the tether point on the Earth's surface

After a point of the tether falls on the surface of the Earth, its motion cannot be described any more by equations (11): in this phase of the motion, one has to take into account, apart from the above forces, the normal reaction of the Earth surface  $\mathbf{R}_i$  and friction force  $\mathbf{F}_{FRi}$ . Equation (1) now becomes

$$m_i \ddot{\mathbf{r}}_i = \mathbf{G}_i + \mathbf{F}_{Ai} + \mathbf{T}_i - \mathbf{T}_{i+1} + \mathbf{R}_i + \mathbf{F}_{FRi} + \mathbf{\Phi}_i^{cf} + \mathbf{\Phi}_i^C. \quad (12)$$

Assume that the Earth surface is spherical; in this case the force of reaction is collinear with the radius-vector of the point:

$$\mathbf{R}_i = R_i \mathbf{r}_i / r_i. \quad (13)$$

Projecting equation (12) onto the direction of the radius-vector, one obtains

$$0 = \frac{(\mathbf{G}_i + \mathbf{F}_{Ai} + \mathbf{T}_i - \mathbf{T}_{i+1} + \mathbf{\Phi}_i^{cf} + \mathbf{\Phi}_i^C) \cdot \mathbf{r}_i}{r_i} + R_i.$$

Therefore

$$R_i = \frac{\mu m_i}{r_i^2} - \frac{F_{Aix} x_i + F_{Aiy} y_i + F_{Aiz} z_i}{r_i} - m_i \omega_E^2 \frac{x_i^2 + y_i^2}{r_i} - 2m_i \omega_E \frac{V_{yi} x_i - V_{xi} y_i}{r_i} - T_i \frac{(x_i - x_{i-1})x_i + (y_i - y_{i-1})y_i + (z_i - z_{i-1})z_i}{r_i \rho_i} + T_{i+1} \frac{(x_{i+1} - x_i)x_i + (y_{i+1} - y_i)y_i + (z_{i+1} - z_i)z_i}{r_i \rho_{i+1}}. \quad (14)$$

The friction force is tangent to the Earth surface; its direction is opposite to the resultant force if the point is in rest and opposite to velocity vector if the point moves:

$$\mathbf{F}_{FRi} = \begin{cases} -\mu_s R_i \mathbf{V}_i, & \text{if } V_i \neq 0; \\ -\mu_r R_i \mathbf{F}_{\perp i}, & \text{if } V_i = 0. \end{cases} \quad (15)$$

Substituting (2)-(4), (10), (13), and (15) to (12), one arrives at the system of differential equations for motion of a tether point on the surface of the Earth.

### H. Stationary solutions and the choice of initial conditions

To determine the tether motion by means of the above model, it is necessary to define the initial positions and velocities of the tether segments. It is reasonable to assume that the tether is deployed along the  $Y$  axis. Consider the tether divided in  $N$  segments with equal lengths  $l_i = L_0 / N$  when unstrained. To calculate the positions of points  $P_i$  for the deployed tether, one should put the right hand side of Eq. (11) to zero and obtain stationary coordinates of the points as solutions to the system:

$$\begin{aligned} x_i &= 0, \quad z_i = 0, \quad V_{x_i} = 0, \quad V_{y_i} = 0, \quad V_{z_i} = 0, \\ 0 &= -\frac{\mu m_i}{y_i^2} + T_i - T_{i+1} + m_i \omega_E^2 y_i. \end{aligned}$$

Here  $i = \overline{1, N+1}$ . From the last equation one obtains

$$-\frac{\mu}{y_i^2} + m_i \omega_E^2 y_i + ES_i \left( \frac{y_i - y_{i-1}}{l_0} - 1 \right) - ES_{i+1} \left( \frac{y_{i+1} - y_i}{l_0} - 1 \right) = 0. \quad (16)$$

Since the tether is anchored to the Earth,  $y_0 = R_E$  (here  $R_E$  is the radius of the Earth), and for the last segment  $y_{N+2} = y_{N+1}$ . Now the initial positions of points  $P_i$  for  $i=1, \dots, N$  can be found as solutions to the non-linear system of equations (16).

### III. Simulation of motion of the space elevator after tether rupture

Based on the system of differential equations constructed in the previous section, the program simulator TetherCalc (<http://www.termech.ru/en/tethercalc.html>) has been developed and several numerical experiments have been carried out. To increase the accuracy of simulation in the computing module of the program, the algorithm of additional division of tether in the atmosphere segment has been implemented.

#### A. Parameters of the space elevator

In this paper, the design of the space elevator proposed by Edwards, as the most thoroughly described at the moment, is used [11]. The tether material is chosen to be a carbon nanotubes fiber. Its density is  $1300 \text{ kg/m}^3$ , tensile strength is 130 GPa, and Young's modulus is 630GPa. Edwards considered a multicore tape tether; however, modeling of the dynamics for such tether is extremely difficult for it can twist about the longitudinal axis due to the action of aerodynamic and other disturbing forces. A model with simplified aerodynamic properties, namely, a homogeneous tether with circular cross-section is used here. Edwards suggests using a tape of width from 0.05 m to 0.115 m and thickness of 1.5 micron; the suggested tape profile is presented in Fig. 5 [11]. A tether of equivalent circular section with diameter from  $2.6 \cdot 10^{-4} \text{ m}$  to  $3.8 \cdot 10^{-4} \text{ m}$  is used. The length of the tether is 117000 km, its mass 5000kg. The counterweight is assumed to be the upper stage of a launch vehicle with mass 3500kg. It is also assumed that the points of the tether after touching the surface of the Earth do not slip, but stick to the ground.

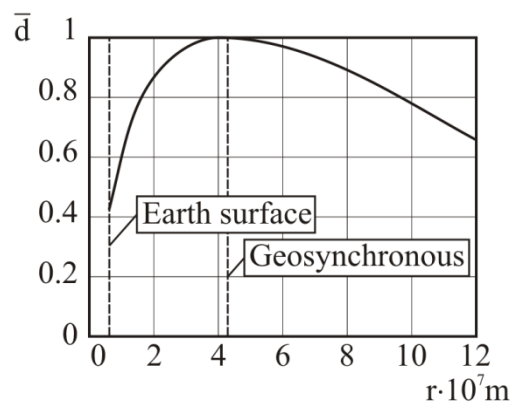
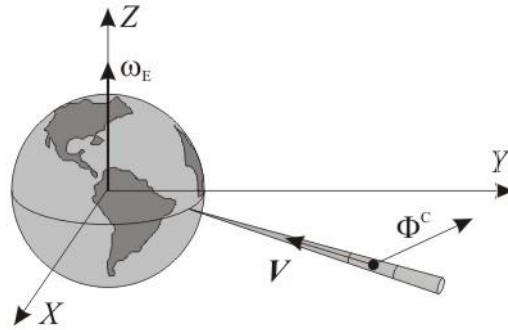


Fig. 5 Tether tape profile

## B. Motion of space elevator without atmosphere influence

Consider a case when tether rupture occurs close to the geostationary orbit. For simulation, the tether is divided into 500 segments of identical length (when unstrained). Numerical simulations show that after rupture the top end of the tether with the counterweight moves away from the Earth, and the lower end moves towards the Earth. Under the influence of the Coriolis force, the tether deviates from the local vertical (Fig. 6) and wraps around the Earth in the direction of its rotation (Fig. 7). If the influence of the atmosphere is not considered, the 40,000 km tether falls to the Earth in approximately 9000 s. More crude modeling with division of the tether in 30 points has not led to qualitative changes of the results.



**Fig. 6 Influence of Coriolis force on tether part motion**

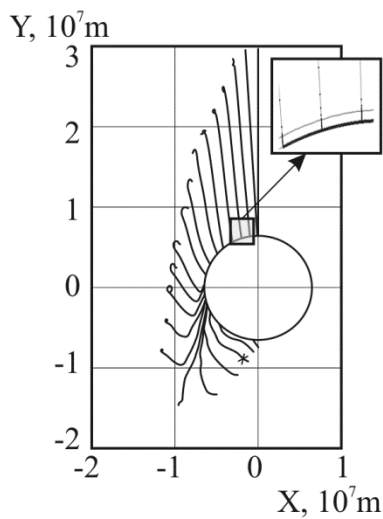


**Fig. 7 Motion of the lower part of the tether after rupture at a planet without atmosphere**

The calculation of the tension in the tether shows that it does not exceed the strength limit for carbon fibers. If the elevator is made of an already available material with tensile strength approximately 5GPa, the rupture may occur in the final stage, when the tether already has circled almost half of the Earth circumference. If the atmospheric influence is not taken into account, the tether lays down on the surface of the Earth quite regularly.

It is convenient to consider the motion of the upper part of the elevator in the fixed inertial coordinate frame  $OX_iY_iZ_i$  connected to the center of the Earth and coincident with the rotating Greenwich coordinate system  $OXYZ$  at the initial moment of time. In this case, the coordinates and velocities of points in the inertial system are

$$\begin{bmatrix} X_i \\ Y_i \\ Z_i \end{bmatrix} = \begin{bmatrix} \cos \omega_E t & -\sin \omega_E t & 0 \\ \sin \omega_E t & \cos \omega_E t & 0 \\ 0 & 0 & 1 \end{bmatrix} \begin{bmatrix} x_i \\ y_i \\ z_i \end{bmatrix},$$

$$\mathbf{V}_i = \mathbf{V}_e + \mathbf{V}_r, \mathbf{V}_e = \boldsymbol{\omega}_E \times \mathbf{r} = [-Y_i \omega_E, X_i \omega_E, 0]^T, \mathbf{V}_r = \begin{bmatrix} \cos \omega_E t & -\sin \omega_E t & 0 \\ \sin \omega_E t & \cos \omega_E t & 0 \\ 0 & 0 & 1 \end{bmatrix} \begin{bmatrix} V_{xi} \\ V_{yi} \\ V_{zi} \end{bmatrix}.$$

First of all, note that at the instant of rupture the velocities of the tether points are orthogonal to the local vertical. On the other hand, the specific energy of the cut part of the tether is higher than that of the whole elevator. Therefore one can conclude that, whatever the consequent orbit of the upper part is, the position of rupture corresponds to a perigee and so the cut part will never hit the Earth.

If we considered a material point then on the basis of its height and speed it would be possible to draw a conclusion on the type of trajectory, if one compares them to the value of parabolic speed  $V_p = \sqrt{2\mu/r}$ . If the speed of the point is less than  $V_p$ , it moves on the closed elliptic trajectory; if it surpasses  $V_p$ , the point escapes the Earth on a hyperbolic trajectory. In the case considered here, the center of mass of the elevator's top part has the velocity exceeding the parabolic velocity  $V_p$  [23]. The upper end of the elevator is a large scale structure, and its orbit after breakage is not Keplerian. However, some estimation can still be done. Figure 8 shows the trajectory of the center of mass of the top part of the elevator and the trajectory of a point with equal mass, and position and velocity of the center of mass in the initial moment of time in inertial coordinate system  $OX_iY_iZ_i$ .

As the space elevator rotates around an axis passing through the center of the Earth with angular velocity equal to the angular speed of the Earth, the absolute velocity of the center of mass of the top part  $V_{cm}$  at the moment of breakage can be found as

$$V_{cm} = \omega_E r_{cm} = r_{cm} \sqrt{\mu / r_{GEO}^3}, \quad (17)$$

Comparing (17) with the expression for parabolic velocity, it is possible to estimate the boundary value  $r_{cm}$  as

$$r_{cm} = \sqrt[3]{2} r_{GEO}. \quad (18)$$

If, after rupture, the distance to the center of mass of the top part surpasses (18), this part will escape the Earth on a trajectory close to hyperbolic.

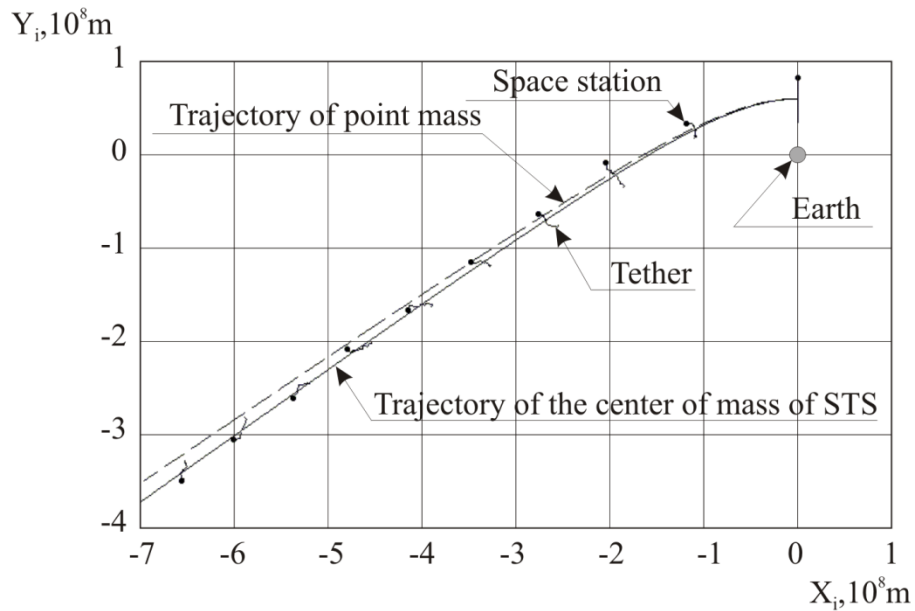


**Fig. 8 Motion of the top part of the space elevator after rupture**

To verify correctness of the numerical model, the energy integral is constructed. As dissipative forces do not act on the top end of the space elevator, the system is conservative and its full mechanical energy should be constant.

Kinetic energy can be found as

$$T = \sum_{i=j}^{N+1} \frac{m_i V_i^2}{2}, \quad (19)$$

where  $j$  is the number of first point of top part of elevator. Potential energy is the sum of potential energy associated with the gravitational field and strain energy of the stretched cable:

$$W = -\sum_{i=j}^{N+1} \frac{\mu m_i}{r_i} + \sum_{i=j+1}^{N+1} \frac{ES_i}{2l_i} (\rho_i - l_i)^2. \quad (20)$$

Time variation of kinetic and potential energy and of their sum are shown in Fig. 9. The total mechanical energy remains constant which testifies that the developed mathematical model does not contradict basic mechanical principles and the result of numerical integration adequately describe the motion.

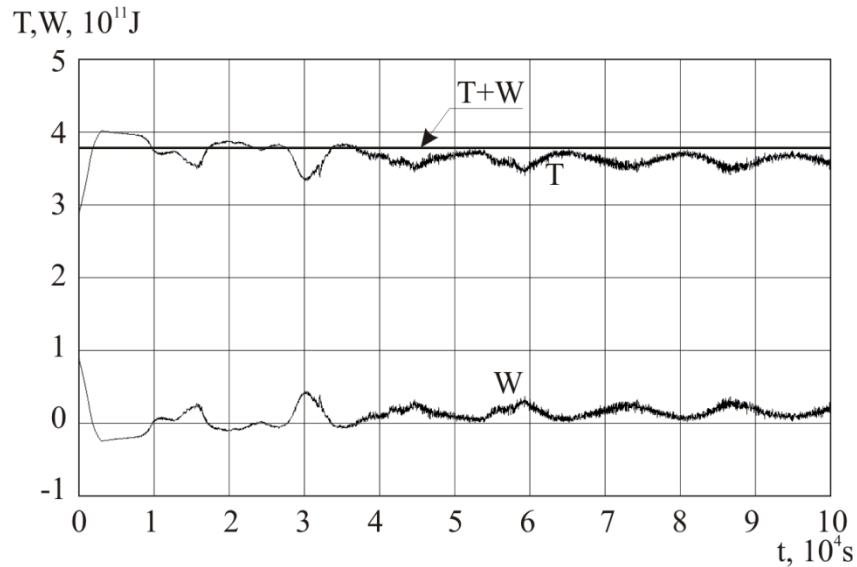


**Fig. 9 Dependences of kinetic, potential and total energy on time**

### C. Motion of the tether in the atmosphere

Influence of the atmosphere change considerably the tether dynamics, leading to quite interesting effects. Since friction force between the tether and the air is not considered, the aerodynamic force does not have a component tangent to the tether segment. This results in damping of the component of the velocity  $V_n$  perpendicular to the respective section of the tether, while the longitudinal component  $V_t$  does not change (Fig. 10). This effect is most pronounced at the initial stage of tether fall when points "slide" along the tether line. The behavior of the tether points is shown in Fig. 11.

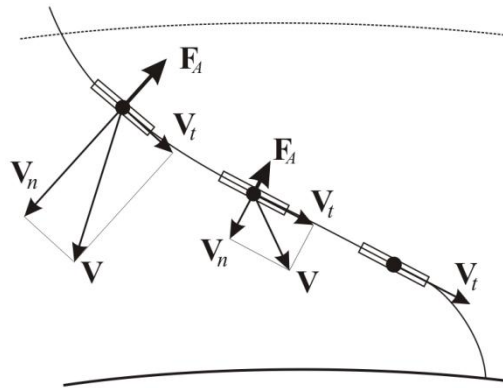


Fig. 10 Damping of the normal component of velocity of the tether's point by aerodynamic force

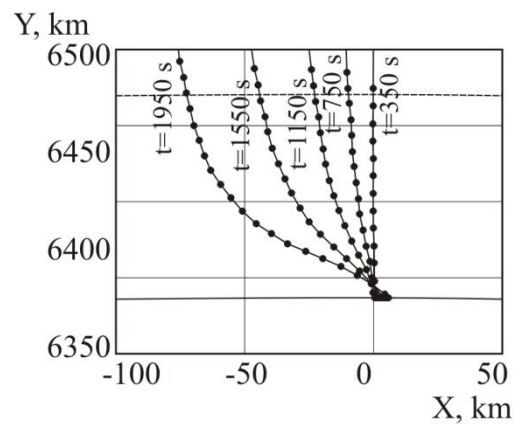
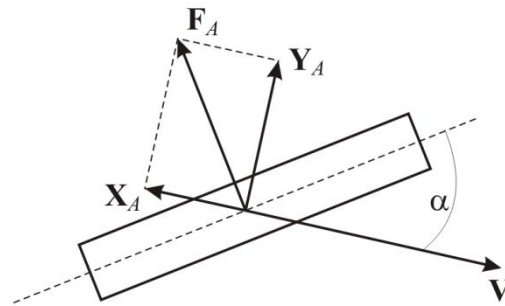


Fig. 11 Tether position at different moments of time

The tether falls to the ground with increasing velocity and the aerodynamic force is proportional to the square of velocity, so the effect of atmosphere on tether motion increases with time. Consider a small element of the tether subject to aerodynamic force that can be decomposed into a lifting force  $\mathbf{Y}_A$  and aerodynamic drag  $\mathbf{X}_A$  (Fig. 12). According to (10), the modulus of aerodynamic force is proportional to the sine of the angle between the longitudinal axis of the tether segment and its velocity vector. If this angle is close to  $\pi/2$ , the motion of the tether section is strongly influenced by the aerodynamic drag which tends to reduce the velocity. In this case, the tether wraps around the Earth unevenly, slowing down in the atmosphere.



**Fig. 12 The aerodynamic force acting on the tether element**

If the angle is small, the lifting force makes significant impact on the motion of the tether segment (Fig. 13a). Under the influence of aerodynamic and Coriolis forces, the tether starts to deviate from the vertical position (Fig. 13b). If its velocity after atmospheric entry remains large enough, the respective part of the tether rises under the influence of the lifting force as though it ricochets from the atmosphere (Fig. 13c), dragging other parts of the tether, which leads to formation of a loop. When its height increases, both the atmospheric density and the aerodynamic force decrease, and the gravitational force becomes predominant. The tether turns downwards and the loop falls to the Earth (Fig. 13d).

The described phenomena is illustrated in Figure 14 that shows the tether at  $t=3500s$ . One can identify parts of the tether with different types of behavior: a loop leaving atmosphere, intervals of smooth descent, and also the parts that reach the ground with rather large velocity.

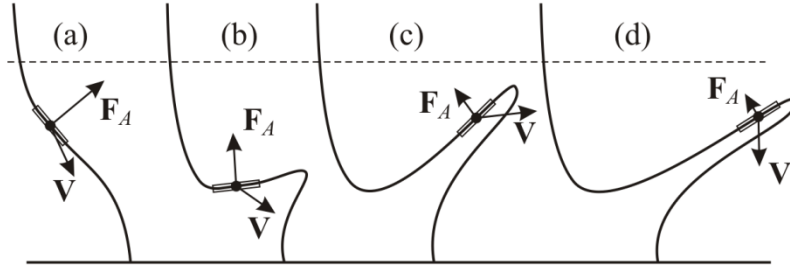


**Fig. 13 Formation of a loop**

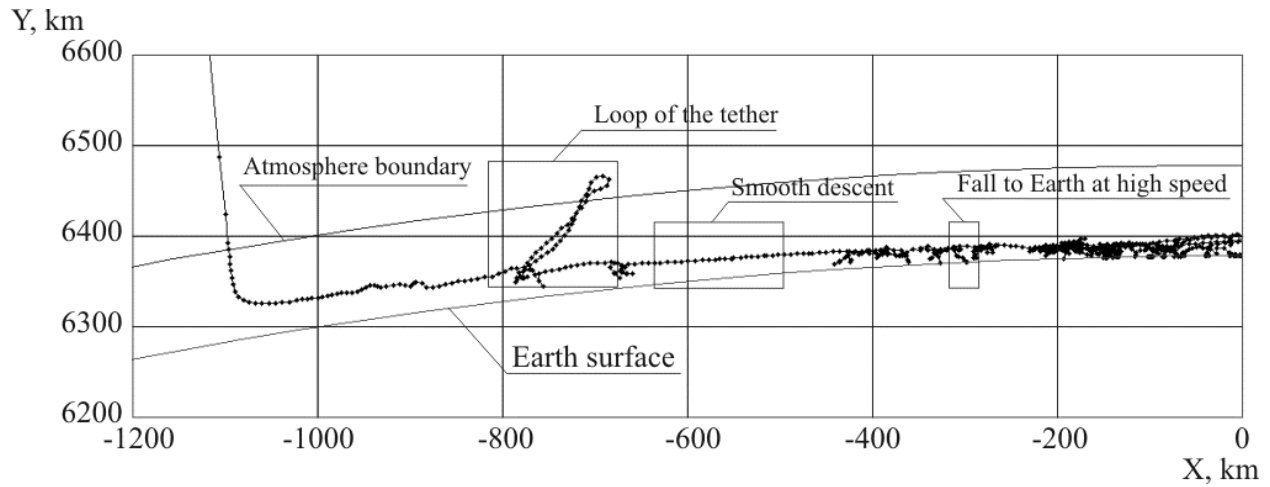


**Fig. 14 Profile of the tether at t=3500s**

#### IV. Conclusions

Analysis of space elevator dynamics after failure presented here shows that the problem is rather complex and worth studying in detail. We focus on the case when the tether is destroyed by space debris in the vicinity of the geostationary orbit, and consider motion of the upper and lower parts of the system after rupture. The mathematical model developed for this purpose represents the flexible heavy tether of circular cross-section as a set of massive points connected by massless viscoelastic bars. The model takes into account the interaction of the tether with the Earth atmosphere during the fall. The approximate expression (18) for boundary value of distance to the center of mass of the top part was obtained. If the distance to the center of mass of the upper part surpasses the boundary value, this part will escape the Earth on a trajectory close to hyperbolic. For lower part numerical simulations show that the aerodynamic force changes significantly the tether behavior. After the tether enters the atmosphere, most of

it slows down and falls smoothly; however, one can notice also quite unexpected motions, such as formation of large loops that can get out the atmosphere. Analysis reveals that some segments of the tether reach the ground with rather large velocities. One can conclude that the rupture of the space elevator ribbon can jeopardize both spacecraft and objects on the Earth's surface located close to the equatorial plane.

### Acknowledgments

This work is funded by the Russian Foundation for Basic Research, project no. 12-01-00317-a. It is also partially supported by the Portuguese Foundation for Science and Technologies (FCT), the Portuguese Operational Programme for Competitiveness Factors (COMPETE), the Portuguese Strategic Reference Framework (QREN), and the European Regional Development Fund (FEDER).

### References

- [1] Swan, P.A., and Penny, R., "Cosmic Study Overview – Space Elevator Feasibility," Proc. of the 63<sup>rd</sup> International Astronautical Congress, Naples, Italy, October 1-6, 2012, IAC-12-D.4.3.01.
- [2] Tsuchida, A., and Allison, A., "Space Elevator Road Map 2011," 62nd International Astronautical Congress, Cape Town, SA, October 3-8, 2011, Paper IAC-11.D4.4.1.
- [3] Beletsky, V.V., and Levin, E.M., "Dynamics of Space Tether Systems," Advances in the Astronautical Sciences, Vol. 83, American Astronautical Society, Springfield, VA, 1993.
- [4] Yu. Artsutanov, "*V Kosmos na Elektrovoze* [To the Cosmos by Electric Train]," Komsomolskaya Pravda, July 31, 1960, (in Russian, see translation, e.g., at [http://www.spaceelevator.com/docs/Artsutanov\\_Pravda\\_SE.pdf](http://www.spaceelevator.com/docs/Artsutanov_Pravda_SE.pdf)).
- [5] Isaacs, J. D., Vine, A.C., Brander, H., and Bachus, G.E., "Satellite Elongation into a True "Sky-Hook," Science, Vol. 151, No. 3711, 1966, pp. 682-683. doi: 10.1126/science.151.3711.682
- [6] Polyakov, G.G., "Generalized problems of the space elevator," Izvesiya AN USSR. Mechanics of Solids, No. 6, 1972, pp.54-59.
- [7] Pearson, J., "The Orbital Tower: A Spacecraft Launcher Using the Earth's Rotational Energy," Acta Astronautica, No. 2, 1975, pp. 785-799. doi:10.1016/0094-5765(75)90021-1.
- [8] Edwards, B.C., "The Space Elevator. NIAC Phase II Final Report," Eureka Scientific, 2003, pp. 42-43.
- [9] Quine, B.M., Seth, R.K., and Zhu, Z.H., "A free-standing space elevator structure: A practical alternative to the space tether," Acta Astronautica, No. 65, 2009, pp. 365-375, doi: 10.1016/j.actaastro.2009.02.018.

- [10] Pugno, N., "On the strength of the carbon nanotube-based space elevator cable: from nanomechanics to megamechanics," *Journal of Physics: Condensed Matter*, №18, 2006, pp. S1971–S1990, doi: 10.1088/0953-8984/18/33/S14.
- [11] Edwards, B.C., "Design and deployment of a space elevator," *Acta Astronautica*, No. 2, 2000, pp. 785–799, doi: 10.1016/S0094-5765(00)00111-9.
- [12] Takeichi, N., "Geostationary station keeping control of a space elevator during initial cable deployment," *Acta Astronautica*, Vol. 70, 2012, pp. 85-94, doi:10.1016/j.actaastro.2011.07.016.
- [13] Woo, P., and Misra, A.K., "Dynamics of a partial space elevator with multiple climbers," *Acta Astronautica*, Vol. 67, 2010, pp. 753–763, doi:10.1016/j.actaastro.2010.04.023
- [14] Williams, P., and Ockels, W., "Climber motion optimization for the tethered space elevator," *Acta Astronautica*, Vol. 66, 2010, pp. 1458–1467, doi:10.1016/j.actaastro.2009.11.003
- [15] Bergamaschi, S., "Tether motion after failure," *Journal of the Astronautical Sciences*, vol. 30, 1982, pp. 49-59.
- [16] Alpatov, A.P., Dranovskii, V.I., Zakrzhevskii, A.E., and Pirozhenko, A.V., "Space tether systems. The problem review," *Cosmic Science and Technology*, Vol. 3, No.5/6, 1997, pp. 21-29. (in Russian)
- [17] Aslanov, V.S., Ledkov, A.S., and Stratilatov, N.R., "Spatial Motion of Space Rope Cargo Transport System," *Scientific and technical journal "Polyot" ("Flight")*, ISSN 1684-1301, No. 2, 2007, pp. 28-33. (in Russian)
- [18] Kruijff, M., and Heide, E.J., "Qualification and in-flight demonstration of a European tether deployment system on YES2," *Acta Astronautica*, Vol. 64, No. 9–10, 2009, pp. 882-905, doi: 10.1016/j.actaastro.2008.10.014.
- [19] Williams, P., "Dynamic multibody modeling for tethered space elevators," *Acta Astronautica*, No. 65, 2009, pp. 399–422, doi: 10.1016/j.actaastro.2008.11.016.
- [20] Tapley, B.D., Watkins, M.M., Ries, J.C., Davis, G.W., Eanes, R.J., Poole, S.R., Rim, H.J., Schutz, B.E., Shum, C.K., Nerem, R.S., Lerch, F.J., Marshall, J.A., Klosko, S.M., Pavlis, N.K., and Williamson, R.G. "The Joint Gravity Model 3", *Journal of Geophysical Research*, No. 101, 1996, pp. 28029-28049.
- [21] Aslanov, V.S., and Ledkov, A.S., "Dynamics of tethered satellite systems," Woodhead Publishing, Cambridge, 2012, pp. 153-160.
- [22] Krasnov, N.F., Koshevoy, V.N., Danilov, A.N., and Zakharchenko, V.F., "Rocket Aerodynamics," Vysshaya Shkola Press, Moscow, 1968, pp 571-579.
- [23] Roy, A.E., "Orbital Motion," IOP Publishing, London, 2005, pp 80-84.